Signatures of a Noise-Induced Quantum Phase Transition in a Mesoscopic Metal Ring

Ning-Hua Tong[2,1] and Matthias Vojta[1]

[1]*Institut für Theorie der Kondensierten Materie, Universität Karlsruhe, 76128 Karlsruhe, Germany*
[2]*Department of Physics, Renmin University of China, Beijing 100872, China*

(Received 22 December 2005; published 7 July 2006)

We study a mesoscopic ring with an inline quantum dot threaded by an Aharonov-Bohm flux. Zero-point fluctuations of the electromagnetic environment capacitively coupled to the ring, with ω^s spectral density, can suppress tunneling through the dot, resulting in a quantum phase transition from an unpolarized to a polarized phase. We show that robust signatures of such a transition can be found in the response of the persistent current in the ring to the external flux as well as to the bias between the dot and the arm. Particular attention is paid to the experimentally relevant cases of Ohmic ($s = 1$) and sub-Ohmic ($s = 1/2$) noise.

DOI: 10.1103/PhysRevLett.97.016802 PACS numbers: 73.23.Ra, 73.23.Hk, 75.40.−s

The persistent current in a mesoscopic ring, penetrated by an Aharonov-Bohm flux, has been studied intensively in the past 20 years [1]. This equilibrium current is an indication of quantum coherent motion of charge carriers in the ring. Recent studies show that the zero-point electromagnetic fluctuations in the leads can suppress quantum coherence and effectively decrease the magnitude of the persistent current [2].

Theoretically, it is known that environmental dissipation can even cause *qualitative* changes in the ground-state properties; i.e., it can drive the system across a quantum phase transition (QPT) into a dissipation-dominated phase. A popular model system is the spin-boson model [3,4], describing a two-level ''impurity'' linearly coupled to a bath of harmonic oscillators. Here a QPT between a delocalized and a localized phase is found for both Ohmic and sub-Ohmic damping [5]. The more complicated Bose-Fermi Kondo model, with an additional fermionic bath, also shows QPT between different ground states [6–9]. Several experiments have been suggested to observe such environment-induced QPT, utilizing single-electron transistors with electromagnetic noise [6,10,11], quantum dots coupled to ferromagnetic leads [7], or cold atoms in optical lattices [12].

In this Letter, we propose to use the persistent current in a metallic ring as a detector of a noise-induced QPT. A suitable setup [2] consists of a ring with a small inline quantum dot, capacitively coupled to an external circuit with dissipative impedance (Fig. 1). The key idea is that tunneling through the barriers can be effectively suppressed by charge fluctuations coupled to the ring electrons. Whereas Ref. [2] studied the magnitude and the fluctuations of the persistent current in the presence of Ohmic noise, we focus here on the QPT caused by the dissipative environment. Modeling the external circuit by a RLC transmission line, we put emphasis on the cases of Ohmic dissipation and a sub-Ohmic dissipation with $\sqrt{\omega}$ spectrum density. They can be realized as LC-dominant and R-dominant limit of the transmission line, respectively [13]. In both cases, we find robust signatures of a QPT between an unpolarized phase at small dissipation and a polarized phase at large dissipation—in the latter, the charge state on the dot is doubly degenerate. Unlike previous proposals for detecting noise-induced QPT, our setup can be realized with either Ohmic or sub-Ohmic dissipation and allows us to assess the influence of finite temperature and bias.

Model.—The setup, shown in Fig. 1, consists of a polarizable environment coupled to the ring-dot system through the capacitors C_d and C_a. For simplicity, we assume spin-polarized electrons; adding the electronic spin degree of freedom would enhance the magnitude of the persistent current [14] but not qualitatively change the physics studied here. Let us first consider the Hamiltonian for charges on the ring and the dot. In a small dot, the level spacing Δ_d will be larger than the tunneling amplitudes t_L and t_R. Regarding the level spacing in the arm Δ_a, we will separately analyze the cases of a small ring $\Delta_a \gg t_L, t_R$ and a large ring $\Delta_a \gg t_L, t_R$. For a small ring, low-temperature charge transport occurs only between the two topmost energy levels of the dot and the arm [2]. This leads to a two-level system $H_{\rm tun} = \frac{\epsilon}{2}\sigma_z - \frac{\Delta}{2}\sigma_x$, with ϵ being the chemical potential difference between the dot and the arm, and $\sigma_{x,z}$ are Pauli matrices. The tunneling

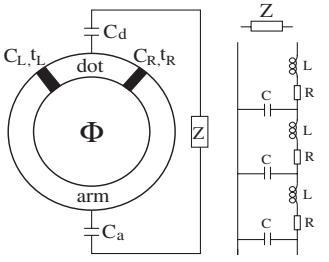

FIG. 1. Ring with an inline dot subject to a flux Φ and capacitively coupled to an external impedance Z. The dot is coupled to the left and right parts of the arm through barriers with tunneling strength t_L and t_R and effective capacitors C_L and C_R. The impedance Z is modeled by an infinite RLC transmission line.

strength is $\Delta = 2\sqrt{t_L^2 + t_R^2 + 2\lambda t_L t_R \cos\varphi}$, where $\varphi = 2\pi\Phi/\Phi_0$ is the external flux in units of the flux quantum $\Phi_0 = hc/e$, and $\lambda = 1\ (-1)$ for an odd (even) number of electrons on the ring. σ_z is related to the charge on the dot by $Q_d = \sigma_z e/2 + (N + 1/2)e$, assuming N permanently occupied states. In the opposite case of a large ring, the energy spectrum in the arm is continuous, and progress can be made via bosonization of the arm electrons. This leads to a coupling between the pseudospin σ_z and the charge density fluctuations in the arm $H_{\rm ohm} = v_F \sum_{k>0} k b_k^\dagger b_k - v_F \sigma_z \sum_{k>0} \sqrt{\pi k/2L}(b_k + b_k^\dagger)$ [10]. It describes an Ohmic bath $J_{\rm ch}(\omega) = 2\pi\alpha_{\rm ch}\omega\Theta(\omega_c - \omega)$, with $\alpha_{\rm ch} = 1/2$. The cutoff is $\omega_c = v_F k_c$, and v_F is the Fermi velocity. In the tunneling part $H_{\rm tun}$, a factor $\sqrt{\rho\omega_c/2\pi}$ now appears in the expression of Δ, where ρ is the density of states at Fermi energy in the arm. Thus, in both the small-ring and large-ring cases we arrive at a two-level system $H_{\rm tun}$ but supplemented with an additional Ohmic bath in the large-ring case.

Now we consider the electromagnetic environment. The RLC transmission line, connecting to the dot and the arm, is described by the distributed resistances R, inductances L, and capacitances C per unit length (Fig. 1). A Hamiltonian description of the environment can be obtained for an effective LC transmission line ($R = 0$). Allowing for an arbitrary distribution of L_n, C_n ($n = 1, 2, \ldots$), the Hamiltonian reads [2] $H_{\rm em} = Q_0^2/(2C_0) + \sum_{n=1}^{\infty}[Q_n^2/(2C_n) + (\phi_n - \phi_{n-1})^2/(2L_n)]$. The impedance is $Z(\omega) = i\omega L_1 + \{i\omega C_1 + [i\omega L_2 + (i\omega C_2 + \ldots)^{-1}]^{-1}\}^{-1}$. Q_0 in $H_{\rm em}$ is the charge on the capacitors C_a and C_d, and $C_0^{-1} = C_a^{-1} + C_d^{-1} + (C_L + C_R)^{-1}$. The operators ϕ_n and Q_n ($n \geq 0$) are conjugate operators satisfying $[\phi_n, Q_m] = \delta_{nm}$. The system-environment coupling originates from the Coulomb interactions, i.e., the charging energy of the capacitors C_L and C_R, $H_{\rm coup} = e/[2(C_L + C_R)]Q_0\sigma_z$. Hence, the full Hamiltonian for the small-ring case reads $H = H_{\rm tun} + H_{\rm coup} + H_{\rm em}$, and for the large-ring case $H = H_{\rm tun} + H_{\rm coup} + H_{\rm em} + H_{\rm Ohm}$.

To study the ground-state properties of H, we use Wilson's numerical renormalization group (NRG) method [15]. NRG is a nonperturbative method for impurity problems and was recently extended to impurity problems with a bosonic bath [16]. We diagonalize the bath degrees of freedom in $H_{\rm em}$ and transform H into the standard form of the spin-boson model

$$H_{\rm sb} = \frac{\epsilon}{2}\sigma_z - \frac{\Delta}{2}\sigma_x + \frac{\sigma_z}{2}\sum_i \lambda_i(a_i^\dagger + a_i) + \sum_i \omega_i a_i^\dagger a_i, \tag{1}$$

with the spectrum $J(\omega) = \pi\sum_i \lambda_i^2 \delta(\omega - \omega_i)$. For the small-ring case, $J(\omega)$ is solely from the electromagnetic contribution $J_{\rm em}(\omega)$ evaluated below. For the large-ring case, $J(\omega) = J_{\rm em}(\omega) + J_{\rm ch}(\omega)$, where $J_{\rm ch}(\omega)$ is from $H_{\rm Ohm}$ as discussed above.

The electromagnetic contribution $J_{\rm em}(\omega)$ is related to the free retarded Green's function of Q_0 as $J_{\rm em}(\omega) = -e^2/(C_L + C_R)^2 {\rm Im}\langle\langle Q_0|Q_0\rangle\rangle_{\omega + i\eta}$. Since $\langle\langle Q_0|Q_0\rangle\rangle_\omega = -1/[i\omega Z(\omega) + C_0^{-1}]$, we have

$$J_{\rm em}(\omega) = -a\omega\, {\rm Re} Z_t(\omega + i\eta). \tag{2}$$

Here $Z_t(\omega) = 1/[Z^{-1}(\omega) + i\omega C_0]$ is the total impedance describing the effective capacitor C_0 in parallel with $Z(\omega)$, and the coefficient $a = [eC_0/(C_L + C_R)]^2$. For the discrete transmission line in Fig. 1, $Z(\omega)$ is a complicated function, which in the continuum limit simplifies to $Z(\omega) = [(R + i\omega L)/i\omega C]^{1/2}$ [13]. In both cases, the asymptotic behavior of $J_{\rm em}$ is $J_{\rm em} = a\sqrt{R/(2C)}\sqrt{\omega}$ for $\omega \ll R/L,\ 1/\sqrt{LC}$ and $J_{\rm em} = a\sqrt{L/C}\omega$ for $1/\sqrt{LC} \gg \omega \gg R/L$. The crossover energy scale R/L separates the low-energy sub-Ohmic $\sqrt{\omega}$ part from the high-energy Ohmic ω part.

For large resistivity R (R-dominant leads), the $\sqrt{\omega}$ part of the spectrum will dominate the dissipation. In the opposite case (LC-dominant leads), R/L is small, and the linear ω spectrum will be relevant in the experimentally accessible range of energies and temperatures. For either type of the leads, the role of the charge modes in the large-ring case $J_{\rm ch}(\omega) \propto \omega$ is only to renormalize the dissipation arising from $J_{\rm em}(\omega)$ and will not change the quantum critical behavior. We will therefore describe both small-ring and large-ring cases using a "pure" bath with a power-law spectral density $J(\omega) = 2\pi\alpha\omega^s\omega_c^{1-s}\Theta(\omega_c - \omega)$, where the exponent s is determined by $J_{\rm em}(\omega)$. The effective dissipation strength α is from $J_{\rm em}(\omega)$ in the small-ring case and in the large-ring case will be further renormalized by $J_{\rm ch}(\omega)$. ω_c is the effective cutoff and taken as our energy unit.

The circulating persistent current operator is $I_c = (C_R I_L - C_L I_R)/(C_L + C_R)$, where I_L and I_R are operators for particle current through the left and the right tunnel barrier, respectively [17]. Because of $\langle\sigma_y\rangle = 0$, the average displacement current $\langle I_L + I_R\rangle$ through the external loop vanishes, and the expectation value of I_c reads $I = \langle I_L\rangle = -\langle I_R\rangle = I_0\langle\sigma_x\rangle$. $I_0 = -e/2\partial\Delta/\partial\varphi$ is the persistent current in the dissipationless limit.

Phase transition.—For a given experimental configuration, the bath exponent s and the dissipation strength α are fixed. Δ can be tuned in the range $[|t_L - t_R|, t_L + t_R]$ by scanning Φ. The bias ϵ is tunable by a gate voltage on the dot. For both the Ohmic and sub-Ohmic spin-boson models, a quantum critical point $\Delta_c(\alpha)$ separates the localized ($\Delta < \Delta_c$) and delocalized ($\Delta > \Delta_c$) ground states [16]. In terms of the charges on the dot, these are the "polarized" and "unpolarized" states, respectively. Note that $\langle\sigma_z\rangle$ can be viewed as an order parameter for this transition, with $\langle\sigma_z\rangle \neq 0$ in the polarized phase. Whereas in the sub-Ohmic case a Δ_c exists for any α (with $\Delta_c \to 0$ as $\alpha \to 0$), in the Ohmic case $\alpha > 1$ is required for the existence of a localized phase. Experimentally, one can cross the critical point by scanning Φ, provided that $|t_L - t_R| < \Delta_c < t_L + t_R$.

Results.—Our results were obtained via the bosonic NRG for the spin-boson model (2), using NRG parameters $\Lambda = 2$ (logarithmic discretization), $M = 80$ (kept states), and $N_b = 6$ (local boson states) [16]. First, we focus on the ground-state persistent current $I = \langle I_c \rangle$ and its response to Δ. The Δ response is related to $\partial I(\Phi)/\partial\Phi$, which can be directly observed in experiment [18]. With the periodic background I_0 removed, $I/I_0 = \langle \sigma_x \rangle$ increases monotonously as Δ increases and saturates in the large-Δ limit. (Note that $\langle \sigma_x \rangle \neq 0$ in both phases of the spin-boson model.) For the sub-Ohmic bath, $0 < s < 1$, $I/I_0 \propto c(\alpha)\Delta$ in the small-Δ limit, as shown in Fig. 2(a). $c(\alpha)$ increases with decreasing α and diverges in the limit $\alpha \to 0$. For the Ohmic case $s = 1$, our data extrapolated to $\Lambda = 1$ are consistent with the perturbative results $I/I_0 \propto \Delta^{\kappa(\alpha)}$, where $\kappa(\alpha) = \alpha/(1-\alpha)$ for $\alpha < 1/2$ and $\kappa(\alpha) = 1$ for $\alpha \geq 1/2$ [2,4].

Approaching the quantum critical point $\Delta = \Delta_c$, a singular contribution arises: $I/I_0 = (I/I_0)_c + c_{\pm}|\Delta - \Delta_c|^{\theta} + (I/I_0)_{\rm reg}(\Delta - \Delta_c)$. The exponent θ can be related to the longitudinal susceptibility exponent γ_{33} [5,19], defined as $\partial\langle\sigma_z\rangle/\partial\epsilon \propto |\Delta - \Delta_c|^{-\gamma_{33}}$, using hyperscaling (see below), with the result $\theta = \gamma_{33}/s - 1$. Since $\theta > 1$, except for $s = 1/2$, I/I_0 near Δ_c is always dominated by the linear term of regular contribution $(I/I_0)_{\rm reg}$, masking the power law in the raw data. However, the susceptibility $\chi_{11} \equiv \partial\sigma_x/\partial\Delta = \partial(I/I_0)/\partial\Delta$ shows clear singularity in the range $1/3 < s < 0.92$ where $\theta - 1 < 1$. For the R-dominant leads, $s = 1/2$, a kink appears in the I/I_0 curve at Δ_c, manifesting the exponent $\theta = 1$ [19]; see Fig. 2(a). Correspondingly, there is a finite jump at Δ_c in the $\chi_{11}(\Delta)$ curve.

The singular behavior at the QPT can be nicely extracted from the persistent current as a function of the bias ϵ. $I(\epsilon)$ is a decreasing function and $I(0)$ depends on both α and Δ. $I(\epsilon)$ has a distinct small-ϵ behavior in the different phases. For $\Delta > \Delta_c$, $I(\epsilon)/I(0) \propto 1 - c\epsilon^2$ with a coefficient c depending on Δ and α; in the decoupled limit $c = 1/(2\Delta^2)$. For $\Delta < \Delta_c$, $I(\epsilon)$ has a finite nonuniversal slope at $\epsilon = 0$. At the critical point $\Delta = \Delta_c$, a power law appears: $1 - I(\epsilon)/I(0) \propto |\epsilon|^{1/\delta_{13}}$. Such distinct behaviors are shown in Fig. 2(b) for $s = 1/2$. For other s values, while the behavior for the delocalized and localized phases is similar, the slope of the critical curve at $\epsilon = 0$ may be zero, a finite value, or divergent, depending on whether $\delta_{13}(s)$ is smaller than, equal to, or larger than unity. The transition point $\delta_{13} = 1$ is at $s = 1/3$ [Fig. 4(a)]. For $s = 1/2$, the exponent $\delta_{13} = 3/2$, leading to a diverging slope of the critical curve [Fig. 2(b)].

To characterize the response of the persistent current to the bias, we introduce a transverse susceptibility $\chi_{13} \equiv -\partial\langle\sigma_x\rangle/\partial\epsilon|_{\epsilon=0} = -(1/I_0)\partial I(\epsilon)/\partial\epsilon|_{\epsilon=0}$. Not only can this quantity be measured from the linear response of the persistent current to the bias, it is also related to the flux induced capacitance $C_\Phi = \partial\langle Q_d\rangle/\partial\Phi$ through $C_\Phi = -e/(2\pi c)I_0\chi_{13}$ [21]. In the delocalized phase $\langle\sigma_z\rangle = 0$, meaning $\chi_{13} = C_\Phi = 0$ for $\Delta > \Delta_c$. χ_{13} is finite for $\Delta < \Delta_c$ and obeys a power law when approaching the quantum critical point from this side, $\chi_{13} \propto (\Delta_c - \Delta)^{-\gamma_{13}}$. γ_{13} is the transverse susceptibility exponent. In Fig. 3(a), we show χ_{13} as a function of Δ/Δ_c for $s = 0.2$ and $s = 0.5$ (symbols with solid lines). Since γ_{13} changes sign at $s = 1/3$, near the critical point χ_{13} approaches zero for $s < 1/3$ while it diverges for $s > 1/3$. This explains the different behavior of $s = 0.2$ and $s = 0.5$ curves in Fig. 3(a).

We examined the above scenario under a finite bias and finite temperatures. As shown in Fig. 3(a) (symbols with dashed lines), a small bias $\epsilon = 0.01$ smears the power-law singularity of χ_{13} and leads to a rounded peak structure in the $\chi_{13}(\Delta)$ curve. The deviation from the zero-bias curve is most prominent near Δ_c. Turning on a finite temperature, χ_{13} are further suppressed on both sides of Δ_c. However, in the regime $T < \epsilon$, the peak structure of χ_{13} curve is always a pronounced feature. This provides a signature of the quantum critical point which is robust against finite bias and finite temperature.

For the LC-dominant leads, $s = 1$, a Kosterlitz-Thouless (KT) transition occurs at a finite Δ_c only for $\alpha > 1$. In this regime, $1 - I(\epsilon)/I(0) \propto c\epsilon$ for both $\Delta < \Delta_c$ and $\Delta = \Delta_c$,

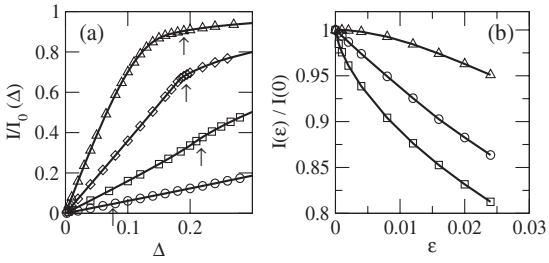

FIG. 2. (a) Rescaled persistent current as function of Δ, for $S = 0.2$, $\alpha = 0.03$; $S = 0.5$, $\alpha = 0.15$; $S = 0.8$, $\alpha = 0.5$; and $S = 1.0$, $\alpha = 1.2$ (from top to bottom). The arrows mark the positions of Δ_c. (b) Rescaled persistent current as function of bias ϵ, at $S = 0.5$, $\alpha = 0.15$ for $\Delta = 0.3$ (triangles), $\Delta = \Delta_c = 0.184\,63$ (squares), and $\Delta = 0.05$ (circles).

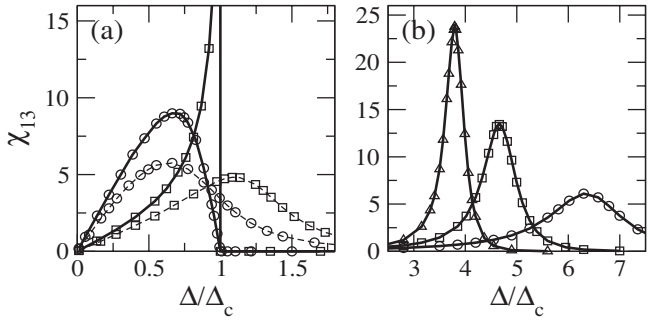

FIG. 3. Susceptibility χ_{13} as function of the rescaled tunneling strength Δ/Δ_c. (a) Sub-Ohmic case: $S = 0.2$, $\alpha = 0.03$ (circles) and $S = 0.5$, $\alpha = 0.15$ (squares). The solid lines are for $\epsilon = 0$ and dashed lines for $\epsilon = 0.01$. (b) Ohmic case: $S = 1$, $\alpha = 1.2$. $\Delta_c \approx 0.0714$. For bias $\epsilon = 10^{-4}$ (dots), $\epsilon = 10^{-6}$ (squares), and $\epsilon = 10^{-8}$ (up triangles), respectively.

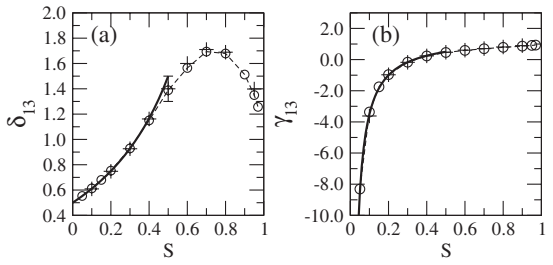

FIG. 4. Critical exponents (a) δ_{13} and (b) γ_{13} (crosses) as function of s, obtained from NRG. Also shown are the hyperscaling results (a) $\gamma_{33}(1+s)/[2(\gamma_{33}-s)]$ and (b) $1-\gamma_{33}(1-s)/(2s)$ (circles with dashed line). The solid lines are the values obtained from hyperscaling relation by setting $\gamma_{33}=1$ in the $s<1/2$ regime [19].

consistent with $\delta_{13}(s=1)=1$ [16]. The transverse susceptibility follows $\chi_{13}\propto\delta(\Delta-\Delta_c)$, instead of the $(\Delta_c-\Delta)^{-1}$ divergence naively expected from $\gamma_{13}\to 1$ as $s\to 1$. In Fig. 3(b), we plot the $\chi_{13}(\Delta)$ curve for $s=1$, $\alpha=1.2$ under a different bias. The peak structure for a finite bias evolves towards a δ peak in the small-ϵ limit. A finite bias shifts the peak position from Δ_c towards larger Δ and broadens the peak dramatically. These χ_{13} curves under finite bias thus present a well-defined precursor of the true QPT at zero bias. For finite temperature $T<\epsilon$, similar peaks are observed with suppressed peak height.

Finally, in Fig. 4 we show the two critical exponents δ_{13} and γ_{13}. A scaling ansatz for the free energy [5] allows one to derive hyperscaling relations between critical exponents, with the results $\delta_{13}=\gamma_{33}(1+s)/[2(\gamma_{33}-s)]$ and $\gamma_{13}=1-\gamma_{33}(1-s)/(2s)$, also shown in Fig. 4 with γ_{33} calculated by NRG. The numerical consistency confirms the validity of hyperscaling in the sub-Ohmic spin-boson model in the entire regime of $0<s<1$ [5]. We also compare the numerical data with the hyperscaling results obtained by setting $\gamma_{33}=1$ for $s\le 1/2$. Within numerical errors, most pronounced at $s=1/2$ due to logarithmic corrections, our data support the analytical result $\gamma_{33}=1$ for $0<s<1/2$ [19,20]. Note that at $s=1/3$, δ_{13} passes one and γ_{13} passes zero, leading to changes in the critical behavior of observables as discussed above.

Let us estimate the parameters in a typical experiment. We take the surface plasma frequency $\omega_p=10^{14}\ \mathrm{s}^{-1}$ as the cutoff energy and energy unit. The upper boundary of the tunable dimensionless Δ is of the order 10^{-3}–10^{-2} [22], and the lower boundary can be very small for a symmetric ring-dot system. The dissipation strength $\alpha_{s=1}\sim 10^{-2}$ and $\alpha_{s=1/2}\sim 10^{-3}$–$10^{-2}$ [13]. For $s=1/2$ (R-dominant leads), this parameter space covers a sufficient region of the phase diagram to make the observation of QPT feasible. For $s=1$ (LC-dominant leads), the α is too small, but the characteristic impedance Z_0 may be increased significantly by optimizing the circuit design and selecting suitable lead materials. Taking into account the $\alpha_{\mathrm{ch}}=1/2$ dissipation from charge fluctuations in the large-ring limit, it is still possible to realize an Ohmic dissipation source with $\alpha>1$ and, hence, to observe the proposed features of the KT transition. For a micron-sized ring, an in-plane magnetic field of 1–10 T will effectively suppress the spin degrees of freedom to realize the spinless electrons employed here.

Summary.—We have identified robust signatures of a QPT, driven by zero-temperature equilibrium environmental noise, in a mesoscopic metal ring. Suitable observables, showing quantum critical behavior, can be derived from the persistent current through the ring. We propose that this system can serve as a tool for studying the noise-induced QPT and probing the low-energy electromagnetic fluctuations in a mesoscopic circuit.

The authors acknowledge helpful discussions with M. Büttiker, R. Bulla, C. H. Chung, S. Florens, R. Narayanan, G. Schön, and A. Shnirman. This research was supported by the DFG through the Graduiertenkolleg GRK 284 (N. H. T.) and the Center for Functional Nanostructures Karlsruhe (M. V.).

[1] M. Büttiker, Y. Imry, and R. Landauer, Phys. Lett. **96A**, 365 (1983).
[2] P. Cedraschi *et al.*, Phys. Rev. Lett. **84**, 346 (2000); Ann. Phys. (N.Y.) **289**, 1 (2001).
[3] A. J. Leggett *et al.*, Rev. Mod. Phys. **59**, 1 (1987).
[4] U. Weiss, *Quantum Dissipative Systems* (World Scientific, Singapore, 1999), 2nd ed.
[5] M. Vojta, N. H. Tong, and R. Bulla, Phys. Rev. Lett. **94**, 070604 (2005).
[6] K. Le Hur, Phys. Rev. Lett. **92**, 196804 (2004).
[7] S. Kirchner *et al.*, cond-mat/0507215.
[8] M. T. Glossop and K. Ingersent, Phys. Rev. Lett. **95**, 067202 (2005).
[9] For references, see M. Vojta, Philos. Mag. **86**, 1807 (2006).
[10] A. Furusaki and K. A. Matveev, Phys. Rev. Lett. **88**, 226404 (2002).
[11] K. Le Hur and M. R. Li, Phys. Rev. B **72**, 073305 (2005).
[12] A. Recati *et al.*, cond-mat/0212413.
[13] G. L. Ingold and Yu. V. Nazarov, in *Single Charge Tunneling*, edited by H. Grabert and M. H. Devoret (Plenum, New York, 1992).
[14] M. Büttiker and C. A. Stafford, Phys. Rev. Lett. **76**, 495 (1996).
[15] K. G. Wilson, Rev. Mod. Phys. **47**, 773 (1975).
[16] R. Bulla, N. H. Tong, and M. Vojta, Phys. Rev. Lett. **91**, 170601 (2003); R. Bulla *et al.*, Phys. Rev. B **71**, 045122 (2005).
[17] P. Cedraschi and M. Büttiker, Phys. Rev. B **63**, 165312 (2001).
[18] R. Deblock *et al.*, Phys. Rev. Lett. **89**, 206803 (2002).
[19] Preliminary analytical results for the spin-boson model [20] show that $\gamma_{33}=1$ in the regime $0<s\le 1/2$.
[20] S. Florens *et al.* (to be published).
[21] M. Büttiker, Phys. Scr. **T54**, 104 (1994).
[22] J. Könemann *et al.*, Phys. Rev. B **73**, 033313 (2006).